Structural principles of B cell antigen receptor assembly

Ying Dong[1,2,7], **Xiong Pi**[1,2,7], **Frauke Bartels-Burgahn**[3,4], **Deniz Saltukoglu**[3,4], **Zhuoyi Liang**[2,5,6], **Jianying Yang**[3,4], **Frederick W. Alt**[2,5,6], **Michael Reth**[3,4], **Hao Wu**[1,2]

[1]Department of Biological Chemistry and Molecular Pharmacology, Harvard Medical School, Boston, MA, USA.

[2]Program in Cellular and Molecular Medicine, Boston Children's Hospital, Boston, MA, USA.

[3]Signaling Research Centers BIOSS and CIBSS, Freiburg, Germany.

[4]Department of Molecular Immunology, Faculty of Biology, University of Freiburg, Freiburg, Germany.

[5]HHMI, Boston Children's Hospital, Boston, MA, USA.

[6]Department of Genetics, Harvard Medical School, Boston, MA, USA.

[7]These authors contributed equally: Ying Dong and Xiong Pi.

Abstract

The B cell antigen receptor (BCR) is composed of a membrane-bound class M, D, G, E or A immunoglobulin for antigen recognition[1-3] and a disulfide-linked Igα (also known as CD79A) and Igβ (also known as CD79B) heterodimer (Igα/β) that functions as the signalling entity through intracellular immunoreceptor tyrosine-based activation motifs (ITAMs)[4,5]. The organizing principle of the BCR remains unknown. Here we report cryo-electron microscopy structures of mouse full-length IgM BCR and its Fab-deleted form. At the ectodomain (ECD), the Igα/β heterodimer mainly uses Igα to associate with Cμ3 and Cμ4 domains of one heavy chain (μHC) while leaving the other heavy chain (μHC′) unbound. The transmembrane domain (TMD) helices of μHC and μHC′ interact with those of the Igα/β heterodimer to form a tight four-helix bundle. The asymmetry at the TMD prevents the recruitment of two Igα/β heterodimers. Notably, the

connecting peptide between the ECD and TMD of μHC intervenes in between those of Igα and Igβ to guide TMD assembly through charge complementarity. Weaker but distinct density for the Igβ ITAM nestles next to the TMD, suggesting potential autoinhibition of ITAM phosphorylation. Interfacial analyses suggest that all BCR classes utilize a general organizational architecture. Our studies provide a structural platform for understanding B cell signalling and designing rational therapies against BCR-mediated diseases.

B cells can recognize structurally diverse antigens, and their antigen receptors play important roles in B cell development and activation. Upon antigen recognition, B cells can be activated and differentiated into plasma cells that secrete antibodies to neutralize the antigens[6-8]. Antigen is bound by membrane-bound immunoglobulin (mIg) as part of the BCR on the B cell surface, as well as by secreted immunoglobulin (sIg or antibody), forms that differ only at the C-terminal end as a result of alternative mRNA processing[9,10]. The different classes or isotypes of mIg and sIg–IgM (μ), IgD (δ), IgG (γ), IgE (ε) and IgA (α)– have different constant regions[1-3]. IgM is the first isotype expressed on all immature and naive mature B cells[11-13]. Similar to the basic architecture of an antibody, mIg comprises a symmetric homodimer of a heterodimer of light chain and membrane-bound heavy chain. The BCR signalling components Igα and Igβ each carry an ITAM at their cytosolic tails[14-16]. Upon antigen recognition, these motifs are phosphorylated by lymphocyte-specific tyrosine kinases, mediating the recruitment of intracellular cofactors to execute the downstream biological effects. In this study, we determined the structural organization of mouse IgM BCR, revealing an implicated mechanism for ITAM autoinhibition.

Structure determination of the IgM BCR

To determine the cryo-electron microscopy (cryo-EM) structure of a BCR, we engineered the mouse myeloma cell line J558L to stably co-express the mIgM heavy chain and a Flag-tagged Igα–YFP fusion, together with endogenous immunoglobulin λ light chain and Igβ (Fig. 1a and Extended Data Fig. 1a). We purified the full-length IgM BCR by anti-Flag affinity and gel filtration chromatography, showing the co-expression of the individual components by SDS–PAGE (Extended Data Fig. 1b-d and Supplementary Fig. 1). Two-dimensional classification (Extended Data Fig. 1e,f) of the cryo-EM data showed large-scale conformational changes at the Fab region owing to the known flexibility at the mIg hinge region[17-20]. The cryo-EM analysis produced a density map with 8.2 Å resolution (Fig. 1b and Extended Data Fig. 1g,h).

To optimize the overall resolution of the BCR structure, we modified the cell line to express a truncated mIgM lacking the two Fab arms (BCR Fab), and purified it using the same procedure as for the BCR (Extended Data Fig. 2a-d and Supplementary Fig. 2). Two-dimensional classification of the cryo-EM data revealed clearer structural features at both the ECD and the TMD compared with the full-length BCR structure (Extended Data Fig. 2e-g). After 3D classification and focused refinement, a homogeneous dataset of around 400,000 particles produced a final map at an overall resolution of 3.3 Å, with best densities at Cμ4, the TMD bundle and part of Igα and Igβ (Fig. 1c, Extended Data Fig. 3 and Extended Data Table 1). We used AlphaFold running on ColabFold notebook[21,22]

to assist with model generation (Extended Data Fig. 4) and density fitting (Extended Data Fig. 5). The final model of BCR Fab includes regions of mIgM from Cμ3 to the TMD and regions of the Igα/β heterodimer up to the TMD (Fig. 1d). Fitting of the BCR Fab structure together with the crystal structures of Fab and Cμ2 domains[23,24] into the density led to the model of full-length IgM BCR (Fig. 1b), and shows that the Fab deletion did not alter the overall structure of the BCR.

The linkers between the ECD and the TMD in mIgM, Igα and Igβ turned out to be important for the organization of the BCR, and we named these the connecting peptides (CPs), following the domain nomenclature used to describe the T cell antigen receptor[25] (TCR). In addition, the 3.3 Å map, as well as an intermediate 3.9 Å map (Extended Data Fig. 3a) also revealed density that we assigned as the ITAM-containing intracellular domain (ICD) of Igβ. Most, but not all side chain densities of the IgM BCR Fab are well defined (Extended Data Fig. 5). In particular, the disulfide bond between Igα and Igβ has little density, suggesting that the bond has been cleaved by radiation damage during cryo-EM data collection; the sensitivity of disulfide bonds to electron beam damage has been observed previously[26].

The ECD interaction within Igα/β

Igα and Igβ ECDs both assume an immunglobulin fold and interact with each other with their β-sandwich domains roughly in parallel (Fig. 2a). Despite the low sequence identity (22%), Igα and Igβ are highly similar in structure, with root mean square deviation of 3.2 Å (Extended Data Fig. 6a). They are related by an approximate two-fold axis (166° in rotation) and linked by a disulfide bond at the interface between two equivalent residues, Igα C113 and Igβ C135 (Fig. 2b,c), which is consistent with a previous prediction[27]. There are five glycosylation sites on Igα and Igβ, all of which have cryo-EM densities for the first *N*-acetylglucosamine (NAG) residue in their *N*-linked glycans (Fig. 2b and Extended Data Fig. 5f). Notably, the glycan on N68 of Igα situates at the interface between Igα, Igβ and mIg, but it is unclear whether it has a role in the assembly of the BCR.

Igα and Igβ interact extensively at the ECD with a buried surface area of around 500 Å^2 each as calculated on the PDBePISA server[28]. Hydrogen bonds are present between Igβ R51 and the carbonyl oxygen atoms of Igα P36 and G114, and between Igβ E138 and Igα S37 (Fig. 2c and Extended Data Fig. 5a). Of note, the packing of the Igα/β heterodimer is distinct from structures of Igβ–Igβ homodimers, which are also linked by the analogous disulfide bond at Igβ C135[27] (Fig. 2d). Residues at the interface between Igα and Igβ are largely conserved across species (Extended Data Fig. 6b,c), suggesting an evolutionarily conserved interaction.

The ECD interaction of Igα/β and mIgM

The Igα/β ECD interacts with the ring-shaped and symmetric Cμ3–Cμ4 dimer of mIgM predominantly on one side, creating an asymmetry in the BCR with μHC proximal and μHC′ distal to Igα/β (Fig. 2a). In this interaction, Igα contributes approximately 830 Å^2 buried surface area, whereas Igβ contributes approximately 90 Å^2. Most of the contacts

are with the Cμ4 domain of μHC with around 750 Å^2 buried surface area, in contrast to 170 Å^2 at Cμ3 (Fig. 2a). The symmetric Cμ3–Cμ4 homodimer aligns well with the cryo-EM structure of sIgM in this region[29,30] (Extended Data Fig. 7a). The mutual interaction between the Igα/β heterodimer and mIgM has an electrostatic component, shown by the largely negatively charged surface of the Cμ4 dimer and the largely positively charged surface of the Igα/β complex (Fig. 2e). In particular, Cμ4 E428 forms an ionic pair with Igα R96 (Fig. 2f). Hydrogen bonds are also present between Cμ4 H424 and Igα Y99, between Cμ4 R429 and Igα N94, and between the Cμ4 G371 carbonyl oxygen atom and Igα S67 (Fig. 2f and Extended Data Fig. 5b). When the TCRβ constant immunglobulin domain of the TCR[25,31] is aligned with the Cμ4 domain of μHC, the CD3ε–CD3γ signalling component of the TCR is situated at the same region as the Igα/β heterodimer, but the TMD arrangements of the two receptors are different (Fig. 2g).

Sequence alignment of the ECDs of different mIg isotypes shows that the key residues involved in the interactions with the Igα/β heterodimer are poorly conserved (Extended Data Fig. 7b). In line with this observation, the isolated ECD of the Igα/β heterodimer binds strongly to a soluble Cμ3–Cμ4 construct of mIgM but barely to analogous constructs from the other isotypes[27]. However, as all mIg isotypes interact with the Igα/β heterodimer, their TMDs may have a dominant role in the assembly of the different BCR isotypes.

The CP interaction of mIgM and Igα/β

The BCR structure shows that the CPs of μHC, μHC′, Igα and Igβ intertwine in a braid-like manner as they connect to the TMD, and may have important roles in the specificity and energetics of BCR assembly (Fig. 3a). There is an apparent crossover by the CPs of Igα and Igβ, resulting in switching of the positions of their ECDs and TMDs (Fig. 3a,b). Of note, similar ECD-to-TMD crossovers are features of all TCR components, including the CD3ε–CD3γ, CD3ε′–CD3δ and TCRαβ complexes[25,31] (Fig. 3b). However, unlike in the TCRαβ complex, the ECDs and TMDs of μHC and μHC′ do not switch positions (Fig. 3a,b). The CP of μHC interacts extensively with Igα/β by intervening between the CPs of Igα and Igβ, whereas the CP of μHC′ interacts only on the outer sides of the CP of Igβ and Cμ4 domain of μHC (Fig. 3b).

The mIgM CP contains a string of acidic residues (Fig. 3a) and displays strong negative electrostatic potential (Fig. 3c). By contrast, the surrounding region from Igα and Igβ, including the CP of Igα is highly positively charged (Fig. 3c). For the CP of μHC, specific salt bridge or hydrogen-bonding interactions may include E436 with μHC′ R340, E442 with Igβ Y112, E443 with Igα K135, and E444 with Igβ R153 (Fig. 3d). For the CP of μHC′, E438 and the carbonyl oxygen of G437 form specific interactions with μHC R340, and E443 mediates a hydrogen bond with Igβ K56 (Fig. 3d). For the CP of Igα, hydrogen bonds are present between R120 and μHC N440, between R125 and Igβ D158, and between E132 and the amide nitrogen of μHC F446 (Fig. 3d and Extended Data Fig. 5c). Collectively, these data suggest that the CPs braid together largely through electrostatic interactions, and that they may be crucial for guiding the assembly of the four-helix bundle in the TMD.

Sequence alignment showed that the CP residues of mIg involved in interaction with Igα and Igβ are less conserved among different isotypes (Extended Data Fig. 7b), which may indicate a diverse role of the CP in BCR assembly. In addition, the CPs of mIg isotypes differ in their lengths. For example, the CP of mIgD contains eight additional residues, and this may be related to the higher stability of the IgD BCR complex compared with the IgM BCR[32].

Assembly of the TMD four-helix bundle

The 4 TMD helices assemble into a tight 4-helix bundle (Fig. 4a and Extended Data Fig. 5d), burying an average of 1,300 $Å^2$ surface area per helix, and thus a massive total surface area of around 5,200 Å. The TMDs of Igα and Igβ differ in their contacts with those of mIgM. Igα contacts TMD helices of both μHC and μHC′, whereas Igβ contacts only that of μHC′ (Fig. 4b). Overall, TMD residues in close proximity with the outer or inner surface of the plasma membrane are often polar or charged, whereas those at the core regions of the helices contain mainly hydrophobic residues (Fig. 4b and Extended Data Fig. 8a-e), consistent with the generic organization of most TMD helices. Charged or polar interactions include those between Igβ Q149 and μHC′ E447, between Igβ K157 and Igα N136, between Igα R137 and μHC N448, and between Igα T140 and μHC T452 (Fig. 4b, left and Extended Data Fig. 5e).

However, the cryo-EM structure reveals that there are also charged or polar residues within the core region of the TMD, especially at the $[E/Q]X_{10}P$ motif on Igα and Igβ[33] (Fig. 4b, right). Notably, Igα E142 in the motif is largely buried within the four-helix bundle and surrounded by hydrophobic residues. Igα E142 is within hydrogen-bonding distance of the equivalent residue Igβ Q164, which may help to dissipate the charge. E142 may also form an anion–aromatic interaction with the conserved mIg residue F456, as the aromatic ring edge is known to exhibit positive electrostatic potential[34,35]. In addition, the hydrophobic environment could potentiate protonation of the E142 carboxylate. We hypothesize that these polar interactions within the membrane may help to precisely assemble the TMD, explaining the relative conservation of Igα E142 across species (Extended Data Fig. 6b) and mIg F456 across isotypes and species (Extended Data Figs. 7b and 8f). The conservation of the charged Igα residue within the membrane is reminiscent of the TCR helical bundle in which charged interactions help to bring the TMD helices together at the centre of the membrane.

Another hydrophilic cluster within the membrane involves S463, Y466 and S467 residues of mIgM that include the YS motif[36,37] (Fig. 4b). Here, hydrogen bonds are formed between two S463 residues and two S467 residues of μHC and μHC′. The Y466 residues of μHC and μHC′ are distant from each other and only μHC Y466 forms a potential hydrogen bond with the main chain amide of Igα G154, and packs against Igα P153, but not the equivalent Igβ P175 residue (Fig. 4b and Extended Data Fig. 5e). In contrast to the poor conservation among different isotypes of mIg at the ECD interaction with the Igα/β heterodimer, high conservation is observed at the TMD domain interaction (Extended Data Figs. 7b and 8f). The TMD helices of μHC and μHC′ are assembled asymmetrically, as shown by their different positioning when superposed by the ECD (Fig. 4c). Consistently, if we add another

Igα/Igβ heterodimer to the empty side of the mIg dimer, the TMD of the heterodimer does not contact the four-helix bundle (Fig. 4d). This lack of interaction at the TMD may explain the 1:1 stoichiometry of the monovalent IgM BCR complex.

ICD density and autoinhibition of ITAM

Since the presumed density for the ICD of Igβ (Fig. 1d) is of low resolution, we used AlphaFold prediction coupled with secondary structure prediction[38] to help with the interpretation of the density. Two short helices around the ITAM motifs appeared to be a consensus among the predictions (Fig. 4e and Extended Data Fig. 9a,b). This observation may be important, as two short helices fit well the cryo-EM density (Fig. 4f). We propose that the helical conformation and the potential foldback onto the end of the Igβ TMD could be autoinhibitory towards ITAM phosphorylation.

Discussion

Our cryo-EM structure of the mouse IgM BCR reveals a 1:1 mIgM:Igα/β complex that is in accordance with previous biochemical and fluorescence resonance energy transfer data[5,39]. The different components of the BCR do not have equal roles in mediating BCR assembly; one of the two mIgM heavy chains (μHC) and Igα have dominant roles in the binding of the Igα/β heterodimer to the mIgM molecule. This explains why the Igα/β heterodimer–but not the previously described Igβ/β homodimer–becomes part of the IgM BCR complex. In addition, the dimeric symmetry of the mIgM ECD is broken by its CPs and TMD. During revision of this Article, cryo-EM structures of human IgM and IgG BCRs were reported[40,41]. Although human and mouse mIgM (excluding the variable domain), Igα, and Igβ share only 60–70% sequence identity, the human and mouse BCR structures are highly similar, suggesting structural conservation across species. Consistent with the structural conservation, a number of previously existing mutations, mainly in the human IgM and IgG BCR, map to our observed interfaces in the mouse IgM BCR (Supplementary Table 1).

The present structure, but not the previous human IgM and IgG BCR structures[40,41], shows density for the ITAM of Igβ, which further suggests a potential auto-inhibited conformation of the ITAM in the resting state. Thus, one potential mechanism for BCR activation may be a conformational change upon antigen binding that overcomes the autoinhibition. However, how antigen binding at the flexibly linked Fab could transmit a conformational change to the ICD remains unknown. A recent structure of the TCR peptide–MHC complex suggested that conformational change of the monomeric TCR complex is an implausible mechanism for TCR activation[31]. An alternative possibility is that antigen binding alters lateral interactions at the BCR, as suggested by the sequence conservation across species on the exposed surface of the IgM BCR, in particular within its TMD (Extended Data Fig. 9c,d). Some of the conserved residues have been shown to involve in inhibitory BCR oligomerization and their mutation results in receptor activation[42]. The conserved residues may also be involved in the binding to other interactors, such as the transmembrane phosphatase CD45 that controls the resting state of T and B cells, and CD19, which is found in close proximity to the IgM BCR only on activated B cells[43]. Our IgM BCR structure provides a starting point for future

structural and functional studies that are required to distinguish between different models of BCR activation upon antigen recognition.

Methods

Construct design

The Flag-Igα-YFP construct encodes a chimeric Igα protein with the Flag tag sequence inserted after the leader peptide of Igα. The cytosolic tail of the chimeric Igα is truncated 10 amino acids after the TMD at G169 and fused with YFP through a RSIATRS linker. The cDNA of the Flag–Igα–YFP construct is cloned into the retroviral vector pMOWS. The expression vector for the truncated IgM BCR Fab (pMS-RL2b) was derived from a pMOWS expressing mouse mIgM heavy chain by replacing the sequence encoding the VH and Cμ1 domains with a Strep tag (WSHPQFEK) connected to the Cμ2 domain via a rigid linker of the sequence A(EAAAK)3A.

Generation of stable cell lines

The mouse J558L cell line expresses endogenous Igβ and λ1 light chain. The cell line J558Lμm15–25 was generated from J558L by stably expressing a mouse mIgM heavy chain with specificity for the hapten 4-hydroxy-5-iodo-3-nitrophenyl acetyl (NIP), and the Flag-Igα-YFP construct. The transfectants were sorted for YFP-positive cells and the expression of a NIP-specific IgM BCR on the cell surface using an allophycocyanin (APC)-coupled 1-NIP peptide and collected by flow cytometry. For the generation of the IgM BCR Fab expressing cell, we transfected the pMS-RL2b vector into the J558L/Flag-Igα-YFP clone 8A1. Before large-scale expression and purification, stable cell lines were further sorted by flow cytometry to collect cells with the high YFP expression.

Flow cytometry

Flow cytometric analysis was used to measure the co-expression of mIgM and Igα/β in IgM BCR and IgM BCR Fab cells. Cells were collected and washed once with PBS. Then, the cells were stained for the surface makers with or without the indicated antibodies (IgM–APC). The APC-IgM antibody was diluted 100 times from stock concentration at room temperature for 5 min. The stained cells were washed once with PBS and resuspended in PBS before flow cytometric analysis. Flow cytometry was performed by Attune Flow Cytometers (Thermo). Attune NxT Software was applied for collecting the data and FlowJo was used to analysing the data. Live cells were gated from the FSC/SSC gate for further analysis. Then, the IgM BCR, IgM BCR Fab cells were gated from GFP and IgM–APC respectively, to show the percentage of the cell populations.

Protein expression and purification

The stable J558L mouse B cell lines were cultured in RPMI 1640 Medium (Gibco, 11875135) with 10% FBS, 100 U ml^{-1} penicillin/streptomycin, 0.05 mM 2-mercaptoethanol, 10 mM HEPES (pH 7.5) and then supplemented with 1.2 mM xanthine (Sigma Aldrich, X-4002), 0.11 mM hypoxanthine (Sigma Aldrich, H9377) and 1 μg ml^{-1} mycophenolic acid (Sigma Aldrich, M3536) for selection of double positive expression. The cells were cultured at 37 °C under 5% CO_2.

Cell pellets from around 10 l suspension culture were subjected to 20 cycles of Dounce homogenization in a low-salt buffer containing 20 mM HEPES pH 7.5, 5% glycerol, EDTA-free protease inhibitor cocktail (Sigma Aldrich, 04693159001) and benzonase nuclease (Sigma Aldrich, E8263). The cell lysate was centrifuged at 42,000 rpm for 1 h (45 Ti fixed-angle rotor, Beckman) at 4 °C.

The cell membrane was transferred to solubilization buffer A containing 20 mM HEPES at pH 7.5, 150 mM NaCl, 5% glycerol, 0.5% lauryl maltose neopentyl glycol (LMNG) with 0.05% cholesteryl hemisuccinate (CHS) (Anatrace, NG310-CH210), EDTA-free protease inhibitor cocktail, followed by 20 cycles of Dounce homogenization and overnight incubation at 4 °C. Membrane solubilization was followed by centrifugation at 42,000 rpm for 45 min at 4 °C to remove the cell debris and insoluble material. The supernatant was incubated with anti-Flag M2 affinity gel (Sigma, A2220) for 6 h. The beads were washed with 20 column volumes (CV) of buffer B containing 20 mM HEPES at pH 7.5, 150 mM NaCl, 5% glycerol, 0.05% LMNG with 0.005% CHS and eluted by buffer C containing 20 mM HEPES at pH 7.5, 150 mM NaCl, 5% glycerol, 0.005% LMNG with 0.0005% CHS and 100 mg ml^{-1} 3× Flag peptide (ApexBio, A6001).

The elution was concentrated to 1 ml by using Amicon Ultra-15 centrifugal filter unit with 100 kDa cut-off (EMD Millipore, UFC910024) and loaded to a step gradient of 10%, 20%, 30% and 40% glycerol in buffer D containing 20 mM HEPES at pH 7.5, 150 mM NaCl, 5% glycerol, 0.005% LMNG with 0.0005% CHS, followed by centrifugation for 16 h at 40,000 rpm (MLS-50 swinging-bucket rotor, Beckman). Fractions with target protein of 1 ml were manually collected and concentrated to 200 μl by using Amicon Ultra-0.5 centrifugal filter unit with 100 kDa cut-off (EMD Millipore, UFC510024). The protein was fractionated by size-exclusion chromatography (Superose 6 increase 5/150, GE Healthcare) with buffer F (20 mM HEPES at pH 7.5, 150 mM NaCl, 0.004% LMNG and 0.0004% CHS) to remove the glycerol.

The purity and quality of the proteins were characterized at all stages of the purification process using 4%–20% SDS–PAGE (Bio-Rad, 4561096) and 3%–12% Bis-Tris gel (ThermoFisher, BN1003BOX). The blue native PAGE (BN-PAGE) was run at 150 V for 1 h first, followed by 250 V for another 1 h at 4 °C. The BN-PAGE buffer contained native PAGE running buffer (ThermoFisher, BN2001) with the addition of a Coomassie Blue-G250 containing cathode buffer additive (ThermoFisher, BN2002). The SDS–PAGE and BN-PAGE were visualized by Coomassie blue staining (Anatrace, GEN-QC-STAIN). The expression of all the components including IgM, Igα and Igβ were visualized by western blotting using anti-mouse IgM mu chain (Abcam, ab97230), anti-mouse λ light chain (Novus Biologicals, NB7552), anti-Flag (Sigma Aldrich, A8592) and anti-CD79B (Santa Cruz Biotechnology, sc-53210) antibodies, respectively.

Negative staining electron microscopy

The peak fractions from gel filtration chromatography were collected and diluted to a final concentration of 0.01 mg ml^{-1} for negative staining electron microscopy. Copper grids with carbon support film (Electron Microscopy Sciences, CF150-CU-UL) were glow discharged for 30 s using a Pelco EasyGlow (Ted Pella) instrument. The sample was applied on freshly

glow-discharged grids and incubated for 1 min and blotted on filter paper to remove excess buffer. The sample was stained by 6 μl 2% uranyl acetate solution (Electron Microscopy Sciences, 22400-2) twice, each for 30 s and blotted again on filter paper. Negatively stained samples were imaged on a Joel JEM1400 Transmission Electron Microscope at 120 keV.

Cryo-EM data collection

The peak fractions from gel filtration chromatography were concentrated to a final concentration of 0.9 mg ml^{-1} and crosslinked by 0.4 mM BS(PEG)5 (Thermo Scientific, A35396) on ice for 40 min before cryo-EM sample preparation. 3.3 μl of the protein samples were placed onto glow-discharged Quantifoil R1.2/1.3, gold grids with 400 mesh (Electron Microscopy Sciences, Q4100AR1.3) before being blotted for 3–3.5 s under 100% humidity at 4 °C and plunged into liquid ethane using a Mark IV Vitrobot (ThermoFisher). Before data collection, all the grids were pre-screened and optimized at Pacific Northwest Center for Cryo-EM at Oregon Health and Science University (PNCC), the University of Massachusetts Cryo-EM Core (UMASS) and Harvard Cryo-EM Center for Structural Biology (HMS) to achieve good ice and particle quality.

Final datasets were collected at HMS using a Titan Krios microscope (ThermoFisher) operating at an acceleration voltage of 300 keV equipped with BioQuantum K3 Imaging Filter (Gatan, slit width 20 eV). Data were collected in two separate sessions. The first session was operated in super resolution mode with 105,000× magnification (0.4125 Å per pixel) and a defocus range between −1.0 and −2.0 μm. For each image stack with 50 frames, the total dose was 55.5 electrons per Å^2. The second session was operated in super resolution mode with 105,000× magnification (0.415 Å^2 per pixel) and a defocus range between −1.0 and −2.0 μm. For each image stack with 60 frames, the total dose was 60.0 electrons per Å^2. SerialEM 3.8 was used for fully automated data collection.

Cryo-EM data processing

The computer support and software for data processing support were provided by SBGrid consortium[44]. For the full-length IgM BCR dataset, raw movies were corrected by gain reference and beam-induced motion by binning twofold with or without dose weighting using the Relion 3.08 implementation of the MotionCor2 algorithm[45]. The motion-corrected micrographs were imported into cryoSPARC[46] to perform blob picking. For the IgM BCR Fab dataset, raw movies were corrected by gain reference and beam-induced motion in the same way as for the full-length IgM BCR dataset. The motion-corrected micrographs were imported into cryoSPARC[46] to perform template picking of 4,496,075 particles using the template generated from the dataset of full-length IgM BCR. Representative 2D classes were then selected as templates for Topaz training[47]. A total number of 3,456,531 particles were picked from a trained Topaz reference resulting in 0.83 per pixel for the individual dataset from two sessions and extracted. Three rounds of 2D classification were performed followed by selecting good particles from good classes. A total of 321,466 particles were selected and merged for further ab initio reconstruction to generate an initial model. These particles from the two sessions were processed similarly for 3D classification into 4 classes. And then the non-uniform refinement with C1 symmetry resulted in 5.9 and 5.4 Å map for two datasets respectively. two classes of 533,389 particles were combined for the final

round of 3D classification into 4 classes. A total of 405,695 particles in total were kept for non-uniform refinement. Additional reconstruction using a tight mask led to maps at 3.9 Å resolution. Local refinement on membrane-proximal region achieved a 3.3 Å final map. All reported resolutions were estimated based on the gold-standard Fourier shell correlation (FSC) = 0.143 criterion. All the cryo-EM maps were corrected and sharpened by applying a negative B factor using automated procedures in RELION 3.1. Local resolution estimation of all the cryo-EM maps were estimated using Phenix[48].

Model fitting and building

We started map interpretation by first building AlphaFold models using the AlphaFold2 implementation in the ColabFold notebooks running on Google Colaboratory[21,22]. Default settings were used with Amber relaxation, and sequences were entered in tandem and separated by a semicolon for prediction of complexes. AlphaFold was run once with each of the 5 trained models, which were checked for consistency. AlphaFold computes pLDDT (predicted local distance difference test, 0–100 with 100 being the best) score to indicate the accuracy of a prediction and we plotted per-residue pLDDT as indication of prediction reliability.

Although several structures of BCR components are available[23,26], there is no structure for any full-length BCR, in particular the full-length structure of the Igα/β heterodimer. To facilitate density interpretation and model building, we first utilized AI-guided protein structure prediction (AlphaFold running on ColabFold notebook)[21,22] to generate models of BCR Fab. The prediction gave good per-residue pLDDT scores at the ECD but poorer ones at the TMD. While the overall prediction showed variability among the five ranked models, the predicted ECD and the TMD of the Igα/β heterodimer are highly consistent, and fitted well with the density individually. By contrast, the interaction between mIgM and the Igα/β heterodimer at either the ECD or the TM were predicted poorly. Thus, we manually placed the mIgM ECD and TMD helices separately and built de novo the flexible CPs between the ECD and TMD for all chains in COOT[49]. The quality of the map was sufficient for sequence assignments for most of the IgM BCR fab complex. Because Cμ2 domain is not visible due to flexibility, the final model of BCR Fab includes the full-length Igα/β heterodimer and Cμ3-TMD of mIgM. For building the full-length BCR, we placed the crystal structures of Fab and Cμ2 domain[23,24] into the density. The cytosolic tail of Igβ containing the ITAM was built as a polyalanine model with two short helices in COOT. Model fitting was conducted using ChimeraX[50]. The BCR Fab structure was refined by real space refinement followed by model validation in Phenix[48]. Because of the modest resolution, hydrogen bonds and salt bridges in the structure were defined by distance cut-offs of 3.5 Å and 4.5 Å, respectively.
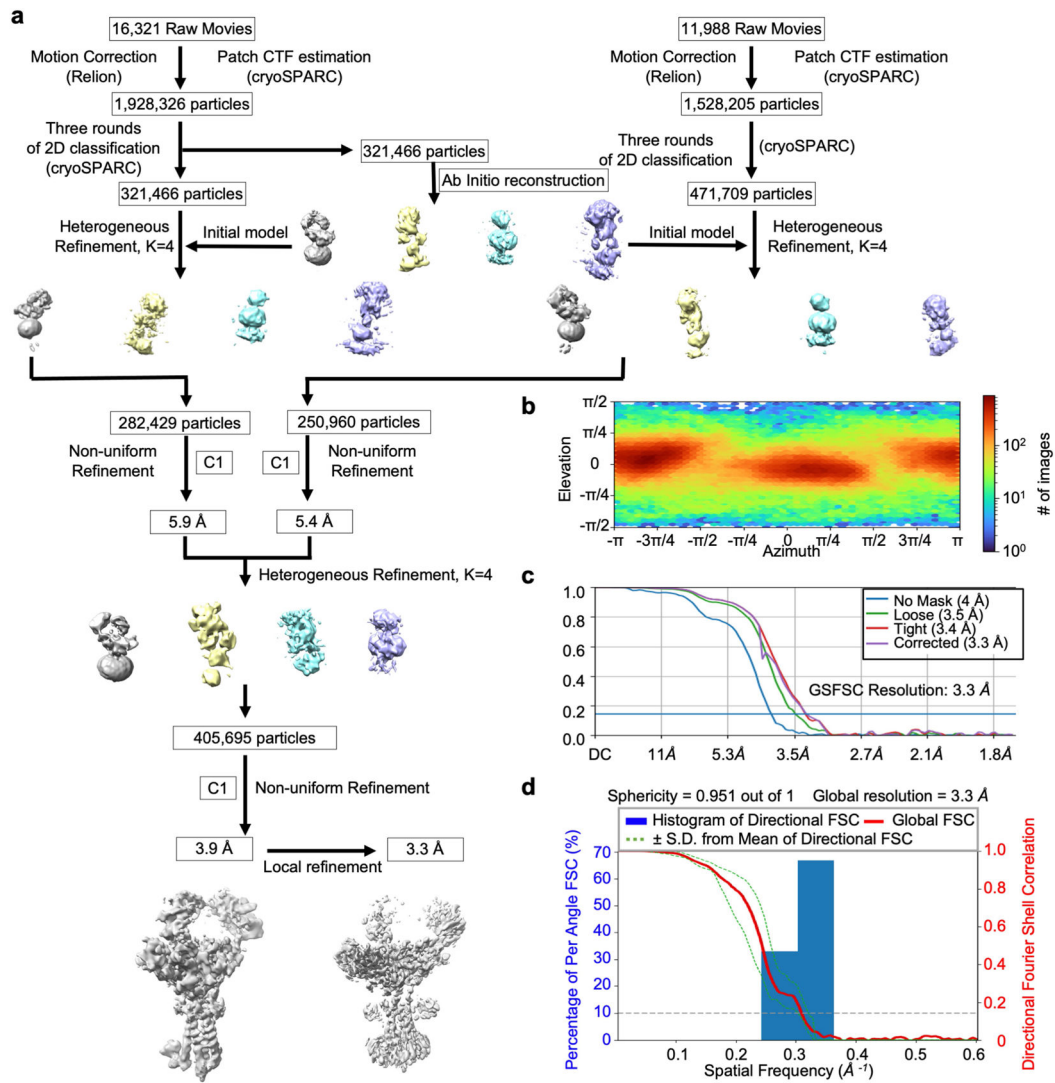
Extended Data
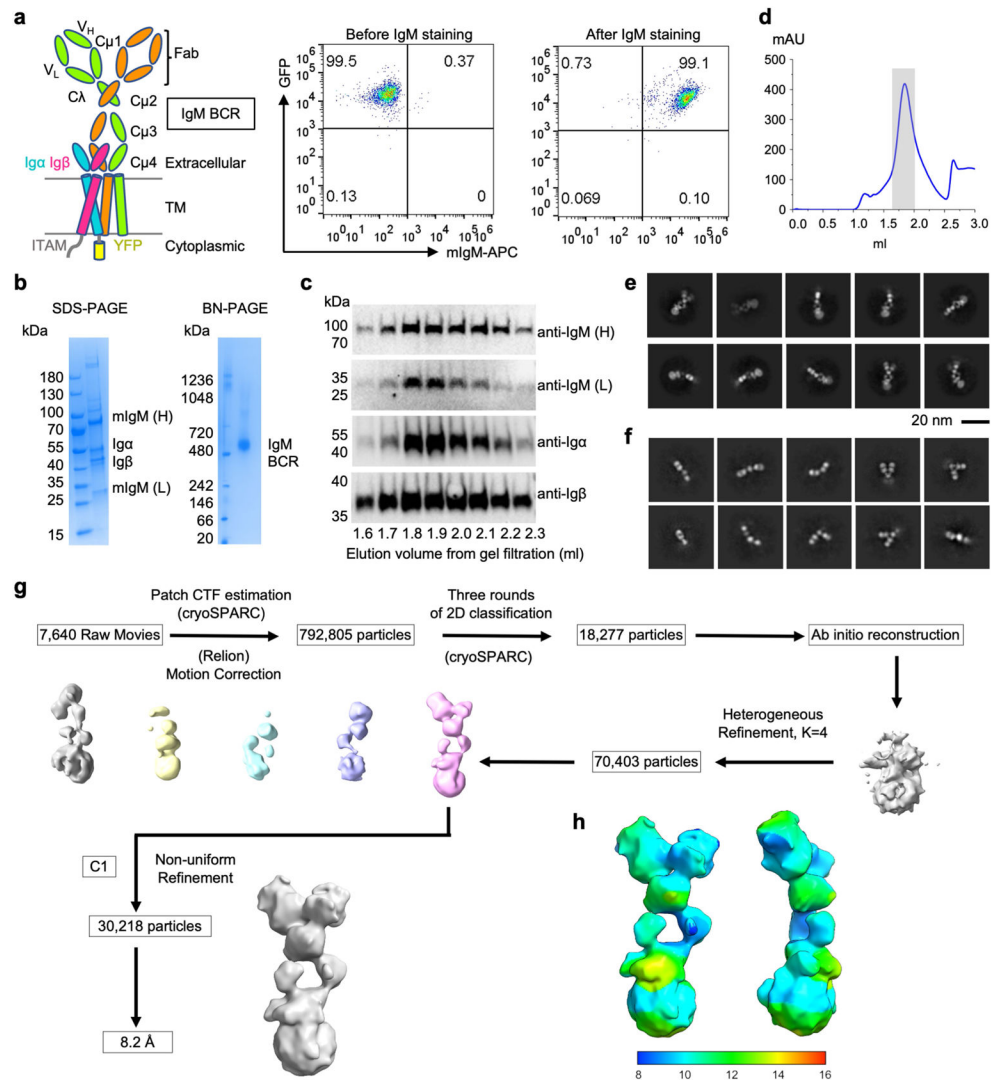
Extended Data Fig. 1 |. Protein purification and cryo-EM data processing of full-length IgM BCR.

a, Selection of J558L B cells that expressed IgM BCR. Domain organization of IgM BCR and surface expression of IgM (APC) and Igα (GFP) by flow cytometry are shown. **b-c**, Purification of IgM BCR shown by SDS-PAGE, Blue-native (BN) PAGE and western blotting using antibodies against the individual subunits. H: heavy chain; L: light chain. **d**, Gel filtration profiles of IgM BCR. The peak of IgM BCR is shaded in grey. **e-f**, Representative 2D classes of IgM BCR (e) and specifically at its Fab region (f). **g-h**, Data processing flow chart (g) and local resolution distribution of IgM BCR (h).
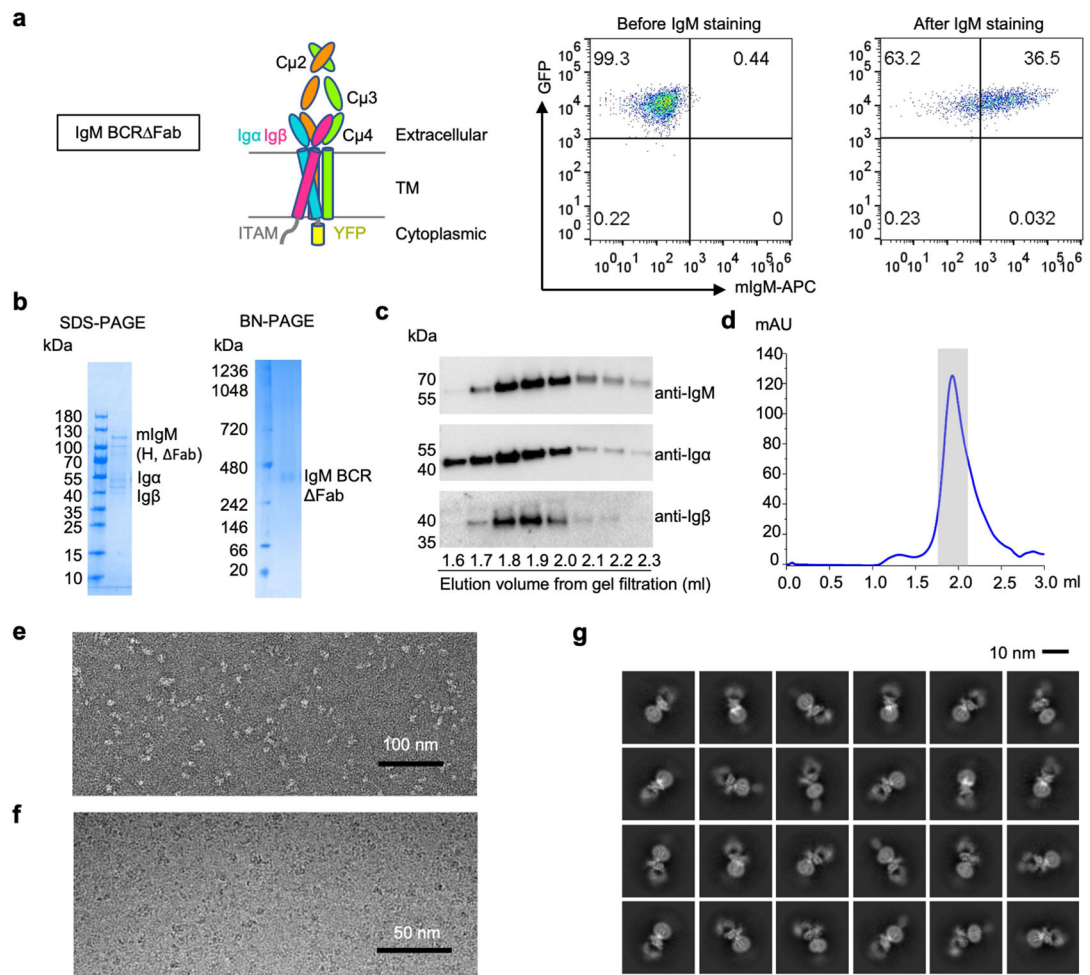
Extended Data Fig. 2 |. Protein purification, raw images and 2D classifications of IgM BCR Fab.
a, Selection of J558L B cells that expressed IgM BCR Fab. Domain organization of IgM BCR Fab and surface expression of IgM (APC) and Igα (GFP) by flow cytometry are shown. **b-c**, Purification of IgM BCR Fab shown by SDS-PAGE, Blue-native (BN) PAGE and western blotting using antibodies against the individual subunits. H: heavy chain. **d**, Gel filtration profiles of IgM BCR Fab. The peak of IgM BCR Fab is shaded in grey **e-f**, Representative negative staining EM image (e) and cryo-EM image of IgM BCR Fab (f). **g**, Representative 2D classes of IgM BCR Fab.

Extended Data Fig. 3 |. Cryo-EM data processing of IgM BCR Fab.
a, Cryo-EM data processing flow chart of the 3.9 Å intermediate cryo-EM map and the 3.3 Å final cryo-EM map of IgM BCR Fab. **b**, Angular distribution of the particles used for the final reconstruction shown as a heat map. **c**, Fourier shell correlation (FSC) plots. **d**, 3D FSC plot.
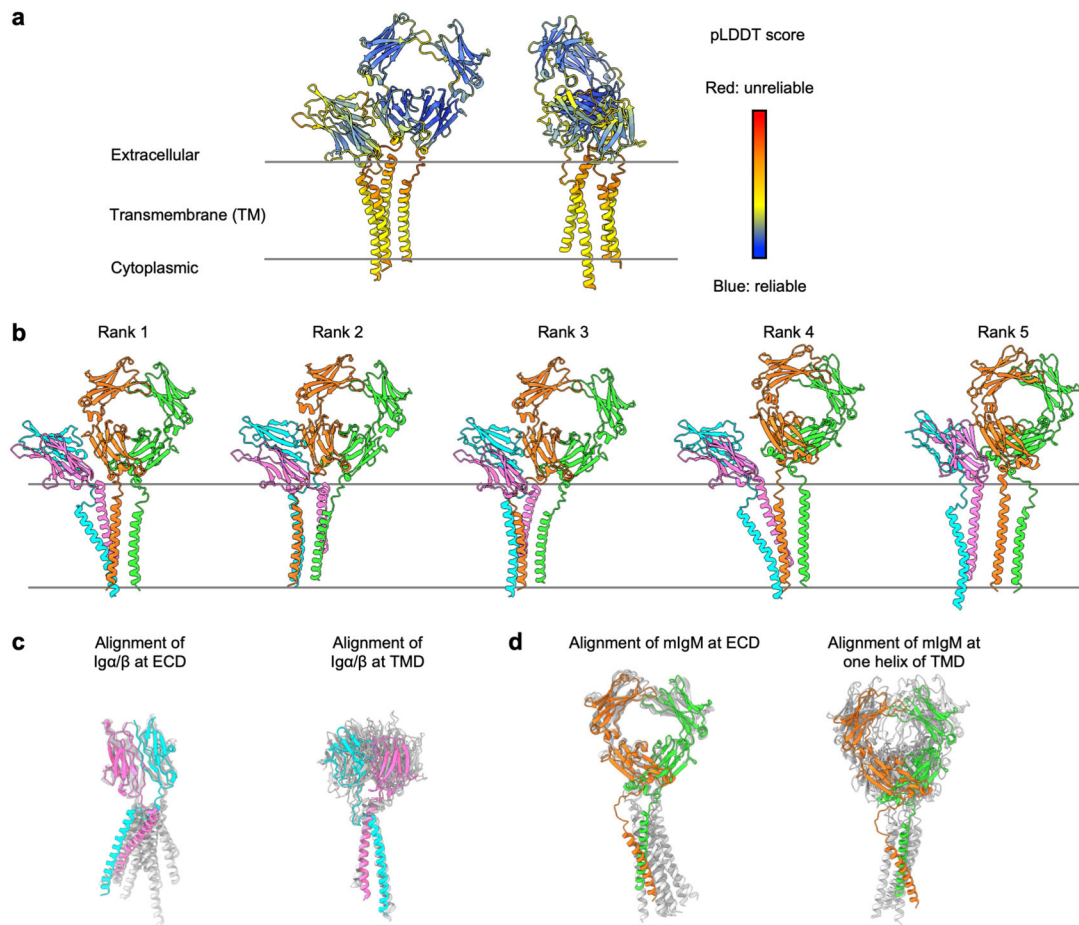
Extended Data Fig. 4 |. AlphaFold predicted models of IgM BCR.
a, The top ranked model of IgM BCR (without Fab and Cμ2) predicted by AlphaFold, coloured by per-residue pLDDT score. **b**, Five predicted models of IgM BCR. **c**, Alignment of the five models of the Igα/β heterodimer at ECD (left) and TMD (right), showing consistent prediction of the ECD interaction (left) and the TMD interaction (right) separately. The CPs of the Igα/β heterodimer were not predicted correctly. **d**, Alignment of the five models of mIgM at ECD (left) and TMD (right) superimposed with IgM BCR Fab model, showing consistent prediction of the ECD interaction (left) but incorrect prediction of the TMD interaction (right). The CPs of the mIgM dimer were not predicted correctly. In (c) and (d), the experimentally determined subunits of the IgM BCR Fab model are shown in their model colours and AlphaFold predicted models are shown in grey.
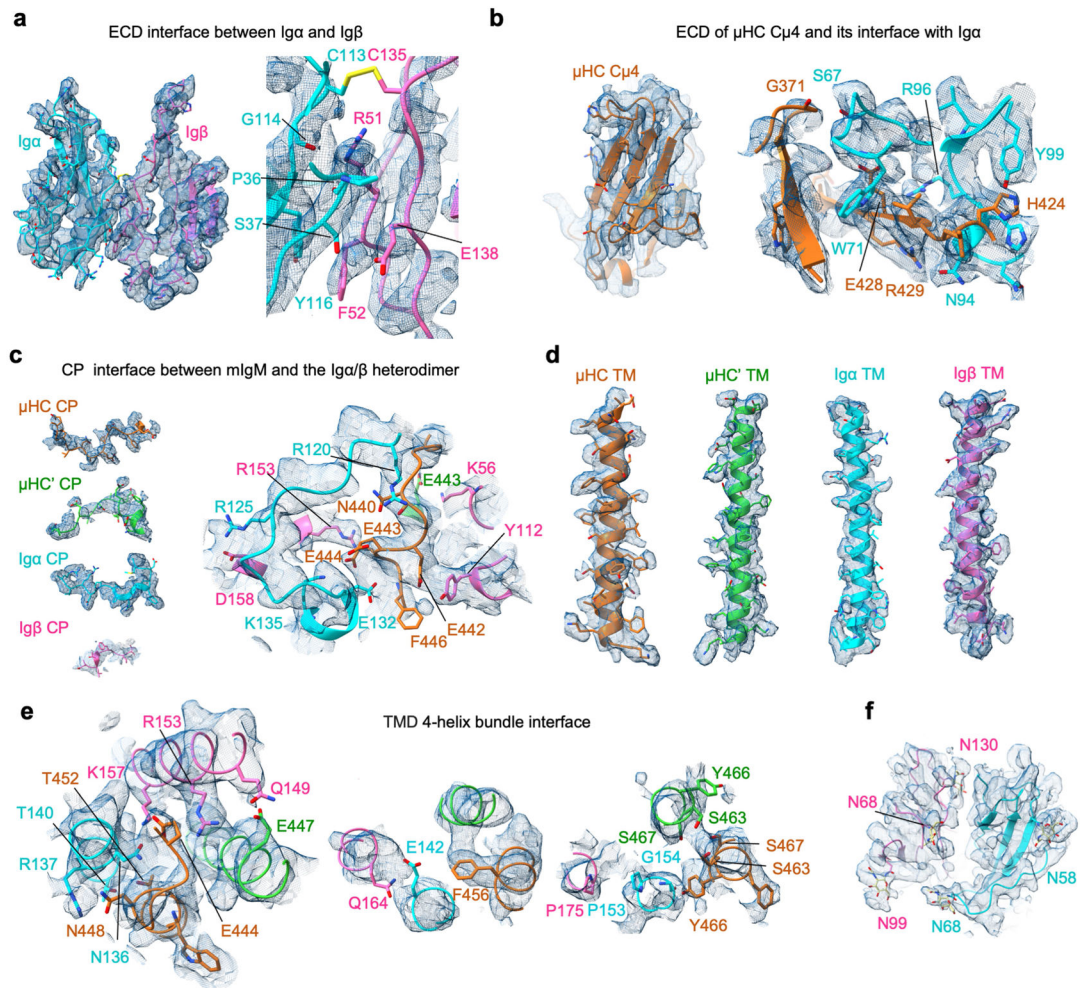
Extended Data Fig. 5 |. Model fitting of IgM BCR Fab in the 3.3 Å cryo-EM map (contour level: 4.0 σ).

a, Ig regions of Igα and Igβ for the Igα/β interaction superimposed with the cryo-EM map. **b**, Interface between μHC Cμ4 and Igα superimposed with the cryo-EM map. **c**, Four connecting peptide regions from μHC, μHC', Igα and Igβ superimposed with the cryo-EM map. Acidic and basic residues are shown and labelled. **d-e**, TMD helices of μHC, μHC′, Igα and Igβ superimposed with the cryo-EM map (d). Key residues mediating the TMD interaction are shown (e). **f**, The fitting of five glycosylation sites on the Igα/Igβ heterodimer.
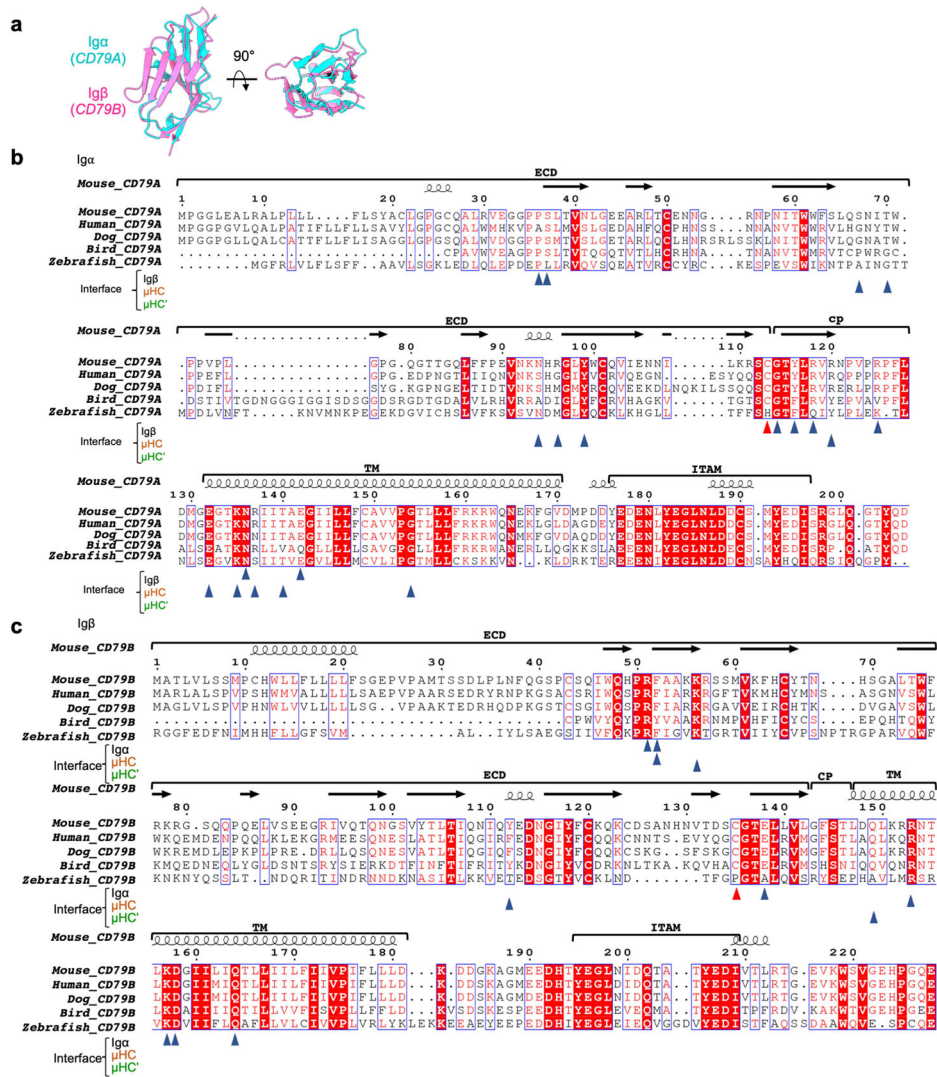
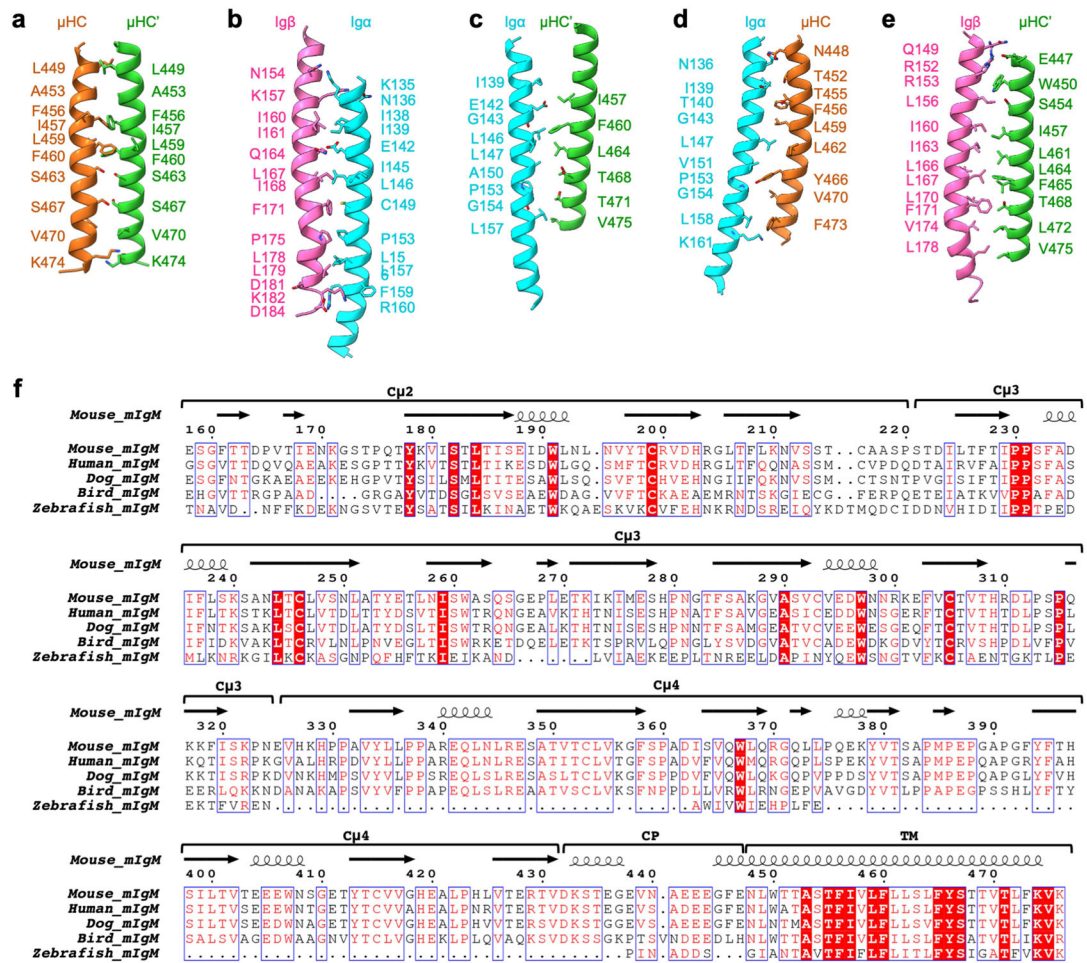**Extended Data Fig. 6 |. Structural and sequence alignment of Igα and Igβ.**
a, Structural alignment between the Ig domains of Igα and Igβ (3.2 Å RMSD). **b-c**, Sequence alignment of Igα (b) and Igβ (c) among different species. Residues at the interface of Igα/β with μHC and μHC' are indicated by triangle symbols. Igα C113 and Igβ C135 are marked by red triangle symbols.
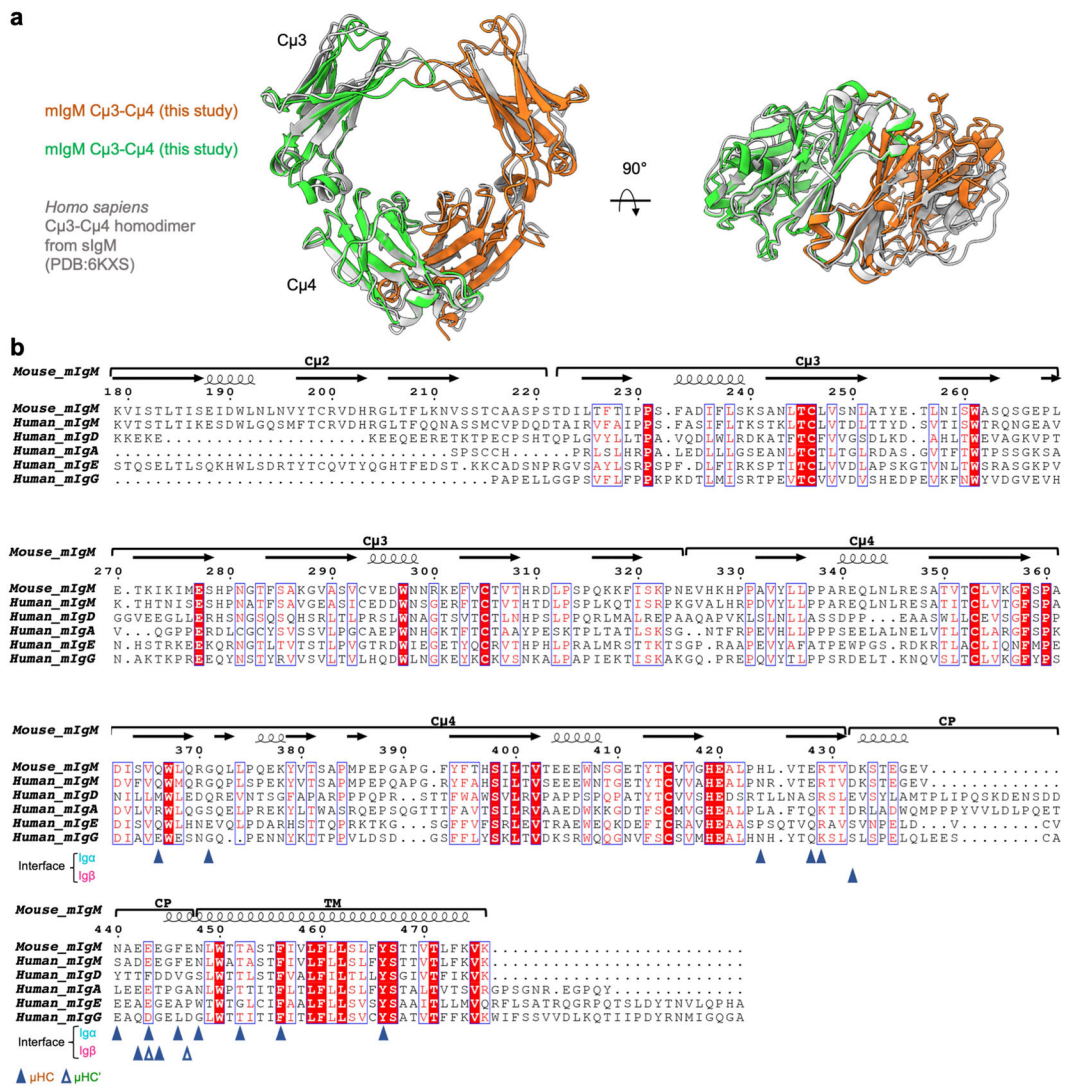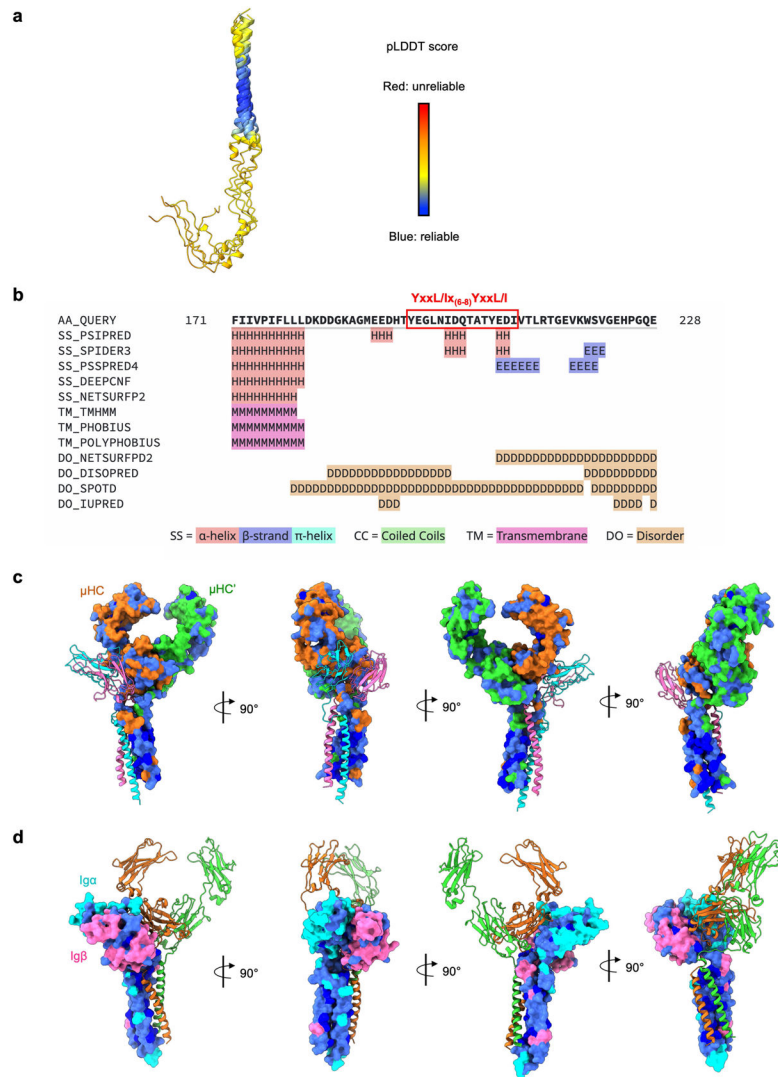
Extended Data Fig. 7 |. Structural and sequence alignment of mIg.
a, Structural alignment of the Cμ3-Cμ4 homodimer of IgM BCR with that from the crystal structure of secreted IgM or sIgM (3.1 Å RMSD, PDB: 6KXS). **b**, Sequence alignment of mIg among different isotypes. Residues at the interface of μHC and μHC' with Igα/β are indicated by solid and hollow triangle symbols respectively.

Extended Data Fig. 8 |. Interaction at TMD and sequence alignment of mIgM.
a–e, The interactions between pairs of helices of TMD. **f**, Sequence alignment of mIgM among different species.

Extended Data Fig. 9 |. AlphaFold prediction and secondary structure prediction of Igβ, and sequence conservation mapping on the IgM-BCR surface.

a, AlphaFold prediction of Igβ. The TMD and ICD of Igβ were predicted, showing the pLDDT scores. **b**, Secondary structure prediction of Igβ (residue 171–228). The ITAM consensus motif is highlighted by red rectangle. **c-d**, Conserved residue distribution on the Cµ3-Cµ4 homodimer surface (c) and the Igα/Igβ heterodimer surface (d) according to sequence alignment among species. The most conserved residues are shown in dark blue, less conserved residues in light blue, and the remaining residues in their chain colours are defined in Fig. 1d.

Extended Data Table 1 |

Data collection, processing, refinement, and validation statistics

Data Collection and Processing	
Microscope	Titan Krios

Voltage (keV)	300
Camera	K3
Magnification	105,000
Pixel size at detector (Å/pixel)	0.83
Total electron exposure ($e^-/Å^2$)	~60
Exposure rate (e^-/pixel/sec)	12.7
Number of frames collected during exposure	60
Defocus range (μm)	−1.0 to −2.0
Automation software	SerialEM 3.8
Energy filter slit width (eV)	20
Micrographs collected (no.)	28,309
Micrographs used (no.)	28,309
Total extracted particles (no.)	793,175
Refinement	
Refined particles (no.) / Final particles (no.)	533,389 / 405,695
Symmetry parameters	C1
Map resolution (Å)	3.3
FSC 0.143 (unmasked / masked)	4.0 / 3.3
Resolution range (Å)	2.8 to 8.8
Resolution range due to anisotropy (Å)	2.8 to 3.1
Map sharpening B factor range ($Å^2$)	−141
Map sharpening methods	LocalDeblur
Model composition	**With / without Cμ3**
Chains	4
Protein residues	805 / 580
Validation	
Model-Map scores	
CC (correlation coefficients)	0.60 / 0.65
Average FSC (0 / 0.143 / 0.5)	(2.6/3.1/7.0) / (2.6/3.1/4.0)
R.m.s. deviations from ideal values	
Bond lengths (Å)	0.005 / 0.005
Bond angles (°)	1.10 / 0.806
MolProbity score	1.90 / 2.11
CaBLAM outliers	3.46 / 4.61
Clashscore	7.22 / 7.84
Poor rotamers (%)	1.41 / 1.94
C-beta outliers (%)	0.00 / 0.00
Ramachandran plot	
Favoured (%)	94.33 / 92.66
Allowed (%)	5.53 / 7.17
Outliers (%)	0.13 / 0.17

Supplementary Material

Refer to Web version on PubMed Central for supplementary material.

Acknowledgements

Data availability

All data and materials reported in the main and supplementary data are available upon reasonable request. The electron density maps of 8.2 Å full-length IgM BCR, 3.3 Å IgM BCR fab and 3.9 Å IgM BCR fab have been deposited in the Electron Microscopy Data Bank (EMDB) with accession codes EMD-27848, EMD-27888 and EMD-28030, respectively. The atomic coordinates for IgM BCR fab and full-length IgM BCR have been deposited in the Protein Data Bank with the accession code of 8E4C and 8EMA.

References

1. Venkitaraman AR, Williams GT, Dariavach P & Neuberger MS The B-cell antigen receptor of the five immunoglobulin classes. Nature 352, 777–781 (1991). [PubMed: 1881434]

2. Alber G, Flaswinkel H, Kim K-M, Weiser P & Reth M in Progress in Immunology Vol. VIII (eds Gergely J et al.) 27–33 (Springer, 1993).

3. Hombach J, Tsubata T, Leclercq L, Stappert H & Reth M Molecular components of the B-cell antigen receptor complex of the lgM class. Nature 343, 760–762 (1990). [PubMed: 2304550]

4. Campbell KS & Cambier JC B lymphocyte antigen receptors (mIg) are non-covalently associated with a disulfide linked, inducibly phosphorylated glycoprotein complex. EMBO J. 9, 441–448 (1990). [PubMed: 2154371]

5. Schamel WWA & Reth M Monomeric and oligomeric complexes of the B cell antigen receptor. Immunity 13, 5–14 (2000). [PubMed: 10933390]

6. McHeyzer-Williams LJ & McHeyzer-Williams MG Antigen-specific memory B cell development. Annu. Rev. Immunol 23, 487–513 (2005). [PubMed: 15771579]

7. Reth M & Wienands J Initiation and processing of signals from the B cell antigen receptor. Annu. Rev. Immunol 15, 453–479 (1997). [PubMed: 9143696]

8. Reth M. Antigen receptors on B lymphocytes. Annu. Rev. Immunol 10, 97–121 (1992). [PubMed: 1591006]

9. Alt FW & Bothwell LM Synthesis of secreted and membrane-bound immunoglobulin mu heavy chains is directed by mRNAs that differ at their 3′ ends. Cell 20, 293–301 (1992).

10. Early P. et al. Two mRNAs can be produced from a single immunoglobulin p gene by alternative RNA processing pathways. Cell 20, 313–3197 (1980). [PubMed: 6771020]

11. Stavnezer J & Schrader CE Ig heavy chain class switch recombination: mechanism and regulation. J. Immunol 193, 5370–5378 (2014). [PubMed: 25411432]

12. Stavnezer J, Guikema JEJ & Schrader CE Mechanism and regulation of class switch recombination. Annu. Rev. Immunol 26, 261–292 (2008). [PubMed: 18370922]

13. Esser C. Immunoglobulin class switching: molecular and cellular analysis. Annu. Rev. Immunol 8, 717–735 (1990). [PubMed: 2188677]

14. Reth M. Antigen receptor tail clue. Nature 338, 383–384 (1989). [PubMed: 2927501]

15. Samelson LE & Klausner RD Tyrosine kinases and tyrosine-based activation motifs. Current research on activation via the T cell antigen receptor. J. Biol. Chem 267, 24913–24916 (1992). [PubMed: 1459994]

16. Flaswinkel H & Reth M Dual role of the tyrosine activation motif of the Ig-alpha protein during signal transduction via the B cell antigen receptor. EMBO J. 13, 83–89 (1994). [PubMed: 8306975]

17. Roux KH, Strelets L, Brekke OH, Sandlie I & Michaelsen TE Comparisons of the ability of human IgG3 hinge mutants, IgM, IgE, and IgA2, to form small immune complexes: a role for flexibility and geometry. J. Immunol 161, 4083–4090 (1998). [PubMed: 9780179]

18. Adlersberg JB The immunoglobulin hinge (interdomain) region. Ric. Clin. Lab 6, 191 (1976). [PubMed: 828971]

19. Sandin S, Öfverstedt L-G, Wikström A-C, Wrange Ö & Skoglund U Structure and flexibility of individual immunoglobulin G molecules in solution. Structure 12, 409–415 (2004). [PubMed: 15016357]

20. Wurzburg BA, Garman SC & Jardetzky TS Structure of the human IgE–Fc Cε3–Cε4 reveals conformational flexibility in the antibody effector domains. Immunity 13, 375–385 (2000). [PubMed: 11021535]

21. Mirdita M. et al. ColabFold—Making protein folding accessible to all. Nat. Methods 19, 679–682 (2022). [PubMed: 35637307]

22. Jumper J. et al. Highly accurate protein structure prediction with AlphaFold. Nature 596, 583–589 (2021). [PubMed: 34265844]

23. Müller R. et al. High-resolution structures of the IgM Fc domains reveal principles of its hexamer formation. Proc. Natl Acad. Sci. USA 110, 10183–10188 (2013). [PubMed: 23733956]

24. Ban N. et al. Structure of an anti-idiotypic Fab against feline peritonitis virus-neutralizing antibody and a comparison with the complexed Fab. FASEB J. 9, 107–114 (1995). [PubMed: 7821749]

25. Dong D. et al. Structural basis of assembly of the human T cell receptor–CD3 complex. Nature 573, 546–552 (2019). [PubMed: 31461748]

26. Kato K. et al. High-resolution cryo-EM structure of photosystem II reveals damage from high-dose electron beams. Commun. Biol 4, 382 (2021). [PubMed: 33753866]

27. Radaev S. et al. Structural and functional studies of Igαβ and its assembly with the B Cell antigen receptor. Structure 18, 934–943 (2010). [PubMed: 20696394]

28. Krissinel E & Henrick K Inference of macromolecular assemblies from crystalline state. J. Mol. Biol 372, 774–797 (2007). [PubMed: 17681537]

29. Li Y. et al. Structural insights into immunoglobulin M. Science 367, 1014–1017 (2020). [PubMed: 32029689]

30. Hiramoto E. et al. The IgM pentamer is an asymmetric pentagon with an open groove that binds the AIM protein. Sci. Adv 4, eaau1199 (2018). [PubMed: 30324136]

31. Sušac L. et al. Structure of a fully assembled tumor-specific T cell receptor ligated by pMHC. Cell 185, 3201–3213.e19 (2022). [PubMed: 35985289]

32. Schamel WWA & Reth M Stability of the B cell antigen receptor complex. Mol. Immunol 37, 253–259 (2000). [PubMed: 10930632]

33. Gottwick C. et al. A symmetric geometry of transmembrane domains inside the B cell antigen receptor complex. Proc. Natl Acad. Sci. USA 116, 13468–13473 (2019). [PubMed: 31209055]

34. Schwans JP et al. Use of anion–aromatic interactions to position the general base in the ketosteroid isomerase active site. Proc. Natl Acad. Sci. USA 110, 11308–11313 (2013). [PubMed: 23798413]

35. Kwong PD et al. Structure of an HIV gp120 envelope glycoprotein in complex with the CD4 receptor and a neutralizing human antibody. Nature 393, 648–659 (1998). [PubMed: 9641677]

36. Parikh VS et al. Differential structure–function requirements of the transmembrane domain of the B cell antigen receptor. J. Exp. Med 176, 1025–1031 (1992). [PubMed: 1402648]

37. Shaw C, Mitchell N, Weaver YK & Abbas AK Mutations of immunoglobulin transmembrane and cytoplasmic domains: effects on intracellular signaling and antigen presentation. Cell 63, 381–392 (1990). [PubMed: 2119890]

38. Zimmermann L. et al. A completely reimplemented MPI bioinformatics toolkit with a new HHpred server at its core. J. Mol. Biol 430, 2237–2243 (2018). [PubMed: 29258817]

39. Tolar P, Sohn HW & Pierce SK The initiation of antigen-induced B cell antigen receptor signaling viewed in living cells by fluorescence resonance energy transfer. Nat. Immunol 6, 1168–1176 (2005). [PubMed: 16200067]

40. Su Q. et al. Cryo-EM structure of the human IgM B cell receptor. Science 337, 875–880 (2022).

41. Ma X. et al. Cryo-EM structures of two human B cell receptor isotypes. Science 377, 880–885 (2022). [PubMed: 35981028]

42. Yang J & Reth M Oligomeric organization of the B-cell antigen receptor on resting cells. Nature 467, 465–469 (2010). [PubMed: 20818374]

43. Gold MR & Reth MG Antigen receptor function in the context of the nanoscale organization of the B cell membrane. Annu. Rev. Immunol 37, 97–123 (2019). [PubMed: 31026412]

44. Morin A. et al. Collaboration gets the most out of software. eLife 2, e01456 (2013). [PubMed: 24040512]

45. Zheng SQ et al. MotionCor2 - anisotropic correction of beam-induced motion for improved cryo-electron microscopy. Nat. Methods 14, 331–332 (2017). [PubMed: 28250466]

46. Punjani A, Rubinstein JL, Fleet DJ & Brubaker MA cryoSPARC: algorithms for rapid unsupervised cryo-EM structure determination. Nat. Methods 14, 290–296 (2017). [PubMed: 28165473]

47. Bepler T. et al. Positive-unlabeled convolutional neural networks for particle picking in cryo-electron micrographs. Nat. Methods 16, 1153–1160 (2019). [PubMed: 31591578]

48. Adams PD et al. PHENIX: a comprehensive Python-based system for macromolecular structure solution. Acta Crystallogr. D 66, 213–221 (2010). [PubMed: 20124702]

49. Emsley P & Cowtan K Coot: model-building tools for molecular graphics. Acta Crystallogr. D 60, 2126–2132 (2004). [PubMed: 15572765]

50. Goddard TD et al. UCSF ChimeraX: meeting modern challenges in visualization and analysis. Protein Sci. 27, 14–25 (2018). [PubMed: 28710774]
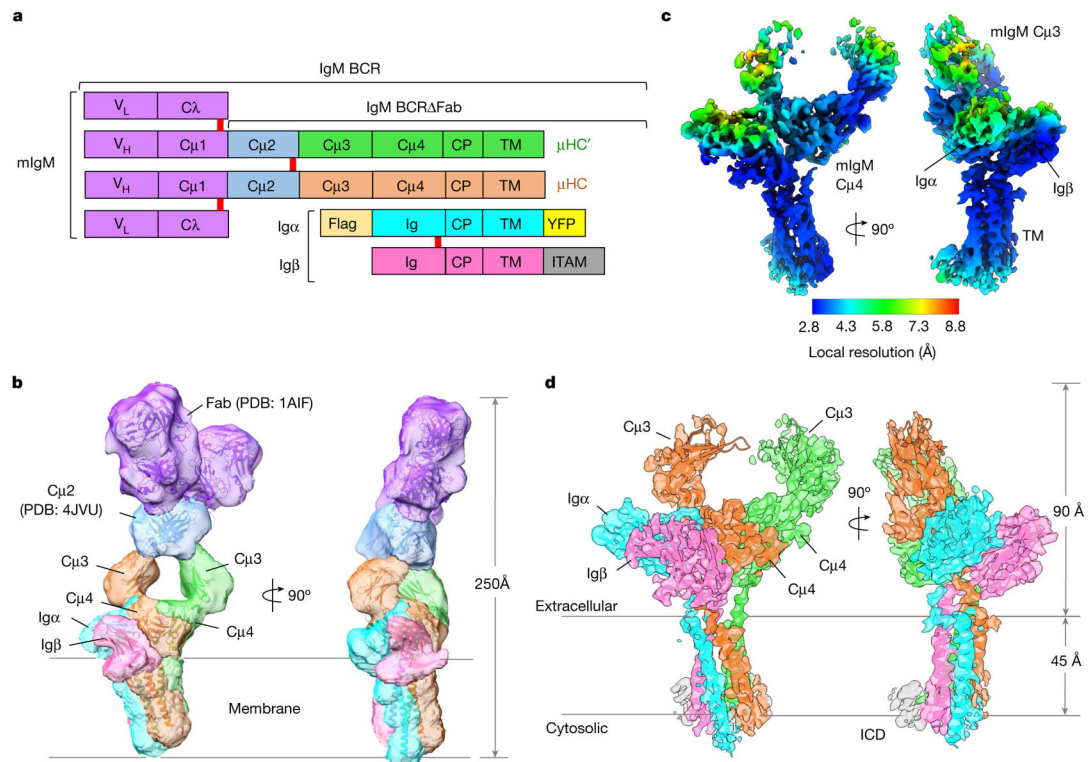
Fig. 1 |. Cryo-EM maps of the IgM BCR.

a, Domain organization of the IgM BCR. Disulfide bonds are shown as red rectangles. mIgM heavy chains μHC and μHC′ are proximal and distal to the Igα/β heterodimer, respectively. CP: connecting peptide. **b**, Cryo-EM map of full-length IgM BCR at 8.2 Å resolution (contour level: 0.5σ) superimposed with the model. **c**, Local resolution distribution of the IgM BCR Fab map at 3.3 Å resolution (contour level: 4.0σ). **d**, Cryo-EM map of IgM BCR Fab (contour level: 4.0σ) superimposed with the model. The Igβ ICD density is shown in grey.
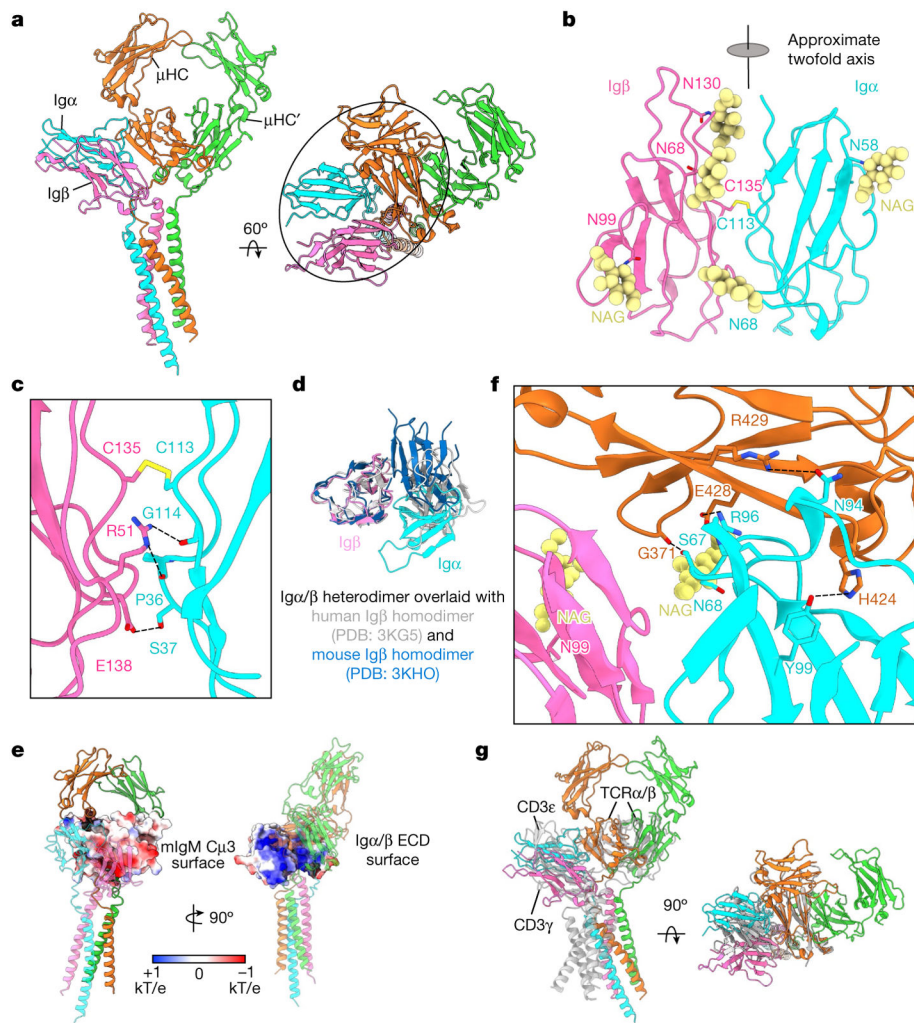
Fig. 2 |. ECD Interactions between the Igα/β heterodimer and mIgM.
a, Ribbon diagrams of the IgM BCR Fab model in different views, with the ECD interactions circled. **b**, Ribbon diagram of the immunglobulin domains of the Igα/β heterodimer. The intersubunit disulfide bond between Igα C113 and Igβ C135 and the observed *N*-linked glycans are shown. The immunglobulin domains of Igα and Igβ are related by an approximate twofold axis. **c**, Detailed interfacial interactions between Igα and Igβ. **d**, Alignment of the immunglobulin domains of the Igα/β heterodimer with two different crystal structures of the Igβ homodimer, showing marked differences. **e**, Electrostatic surfaces (−1 to +1 kT/e) of the interacting Cμ4 (left) and the immunglobulin domains of the Igα/β heterodimer (right). **f**, Detailed interactions between ECD residues of the Igα/β heterodimer and the mIgM molecule. **g**, Alignment of the Cμ4 domain of IgM BCR with the TCRβ constant domain (grey), showing that the immunglobulin domains of the Igα/β and CD3ε–CD3γ (grey, PDB: 6JXR) heterodimers occupy the similar location relative to mIgM and TCRαβ, respectively.
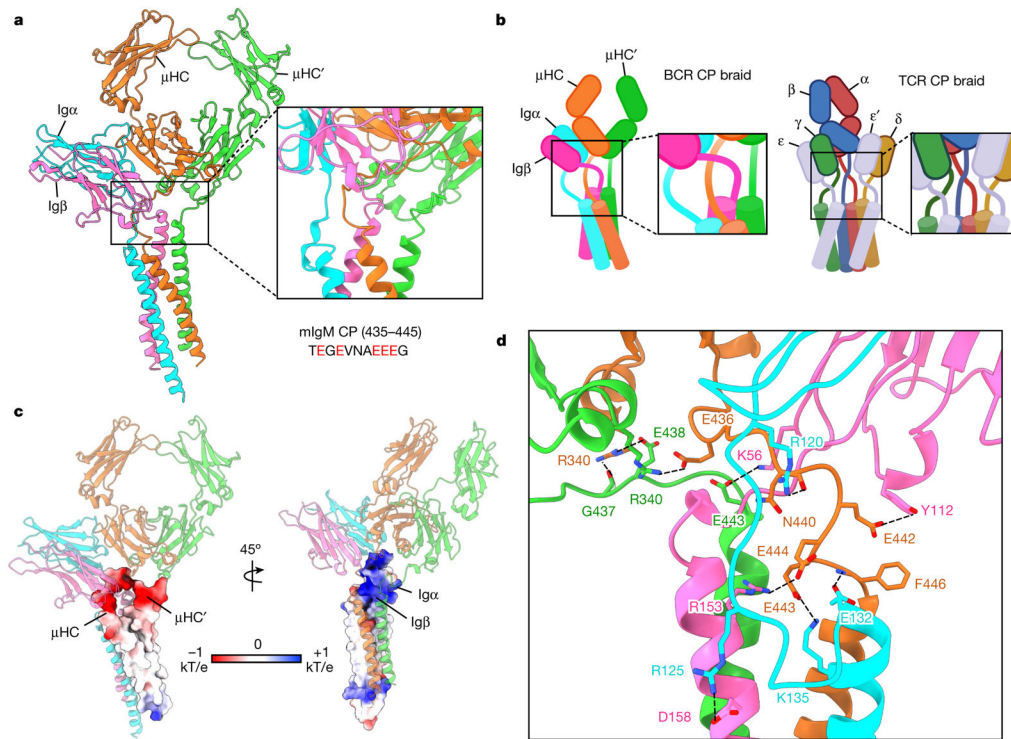
Fig. 3 |. CP interactions between the Igα/β heterodimer and mIgM.
a, Global view (left) and enlarged view (right) of the CP region of IgM BCR, showing the intertwining in this region. The sequence of mouse mIgM CP (435–445) is shown with acidic residues in red. **b**, Schematic diagrams for the CP assembly of BCR (left) and TCR (right). **c**, Electrostatic surfaces (−1 to +1 kT/e) at the CPs of mIgM (left) and the CPs of Igα and Igβ (right). **d**, Detailed interactions between the charged CP residues of the Igα/β heterodimer and mIgM.
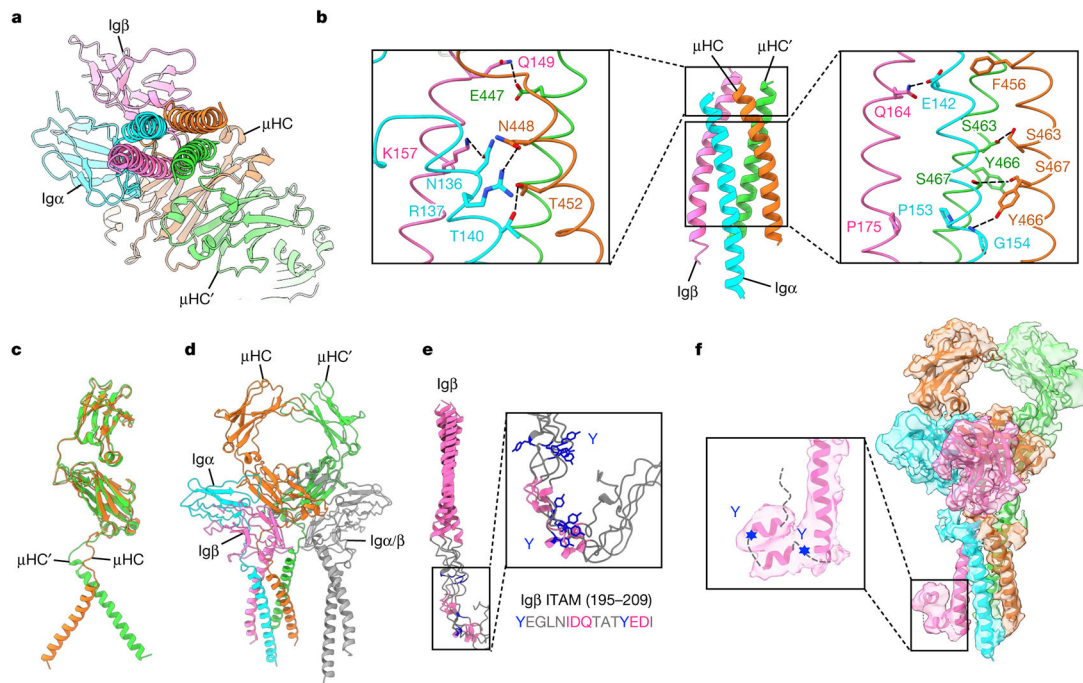
Fig. 4 |. TMD assembly of the IgM BCR.

a, Bottom view of the TMD assembly shown in ribbon. **b**, Key polar interactions at the TMD, including those at the membrane-proximal region (left) and within the membrane including the [E/Q] $X_{10}P$ motif on Igα and Igβ and the YS motif on mIgM (right). **c**, Structural alignment of μHC and μHC′ in an mIgM dimer, showing the different asymmetric conformation at the TMD. **d**, Structural alignment of a second Igα/β heterodimer to the empty side of the mIgM Cμ4 dimer showed the lack of interaction with the four-helix bundle of TMD, which may explain why the second Igα/β heterodimer is not recruited to the BCR. **e**, Ribbon diagrams of five top-ranked models of Igβ TMD and ICD predicted by AlphaFold, shown with a detailed view of the ITAM region. The two tyrosine (Y) residues at the Igβ ITAM (YxxL/lx$_{(6-8)}$YxxL/I motif) and the two predicted short α-helices are shown in blue and pink, respectively. The short α-helices were also identified by secondary structure prediction[37]. **f**, Fitting of an ITAM polyalanine model as an α-helical hairpin into the 3.9 Å intermediate cryo-EM map (contour level, 8.0σ). The hairpin and the foldback onto the Igβ TMD may keep the ITAM in an auto-inhibited form.